Monitoring Welding Torch Position and Posture Using Reversed Electrode Images – Part I: Establishment of the REI-TPA Model

A new method was developed to relate welding torch position and attitude to reversed electrode image on weld pool surface during GTAW

BY Y. FU AND S. B. CHEN

Abstract

Sensing, modeling, and control are the key technologies of intelligent welding manufacturing. The position and attitude of the welding torch relative to the weld seam affects the quality of the produced weld directly, which is the basis of control and offline programming of the welding robot. Based on the existing research of reversed electrode image (REI) on monitoring of weld pool surface and penetration state, this work focused on the application of REI on monitoring of welding torch position and attitude (TPA). In this paper, a REI-TPA model was established to quantitively relate REI to TPA by considering the surface of the weld pool as a spherical mirror. With the REI-TPA model, the offset distance and deflection angle of the welding torch relative to the correct position and attitude can be calculated. The calculation is based on the measurement of the relative distance between the tip of REI and the electrode in a passive visual image of the weld pool, arc length, and weld pool geometry. This model can be applied to the real-time control of TPA, which is a supplement to the application of welding passive visual image and an extension to multi-information acquisition and processing methods in the robotic welding process.

Keywords

- Passive Vision
- Reversed Electrode Image
- Position and Attitude of Welding Torch

https://doi.org/10.29391/2024.103.019

Introduction

Sensing, modeling, and control are the key technologies of intelligent welding manufacturing (Refs. 1–3). The position and attitude of the welding torch (TPA) relative to the weld seam is of vital importance to the realization of intelligent welding manufacture, which is the basis of the arc welding robot control and offline programming, directly affecting the quality of the produced weld. A skilled welder can adjust TPA in real time with visual information during welding. Similarly, automatic detection and correction of TPA can be realized by establishing a quantitative model between TPA and the image of the weld pool.

At present, the main method to monitor the pose of the welding torch is to use various sensors, such as an inertial measuring unit (IMU), rotating arc sensor, angle sensor, etc. Zhang et al. (Refs. 4, 5) measured the torch attitude using a wire IMU during gas tungsten arc welding (GTAW). According to the improved quaternion-based unscented Kalman filter, the error of the obtained torch attitude was in the order of 1 deg (X-axis and Y-axis) and 2 deg (Z-axis). Le et al. (Ref. 6) established a rectangular filler weld tracking system, and a mathematical model of the torch posture was established based on the rotation arc sensor. While these methods have certain limitations: the IMU system has a complex structure; with an angle sensor and rotation arc sensor, only partial deflection of the welding torch can be monitored.

In 2017, Chen et al. (Refs. 7, 8) defined and extracted the reversed electrode image (REI) in a passive vision image of the weld pool collected in GTAW. A reflection model was proposed to calculate the surface height (SH) of the weld pool with REI. The penetration state was then predicted using the derivative of the SH. The creatively proposed REI was an important expansion to the welding multi-information system. The new feature of REI can be widely applied to the monitoring and control of the welding process, which was of significance to the seam tracking and adjustment of position and attitude of the welding torch during the robotic welding

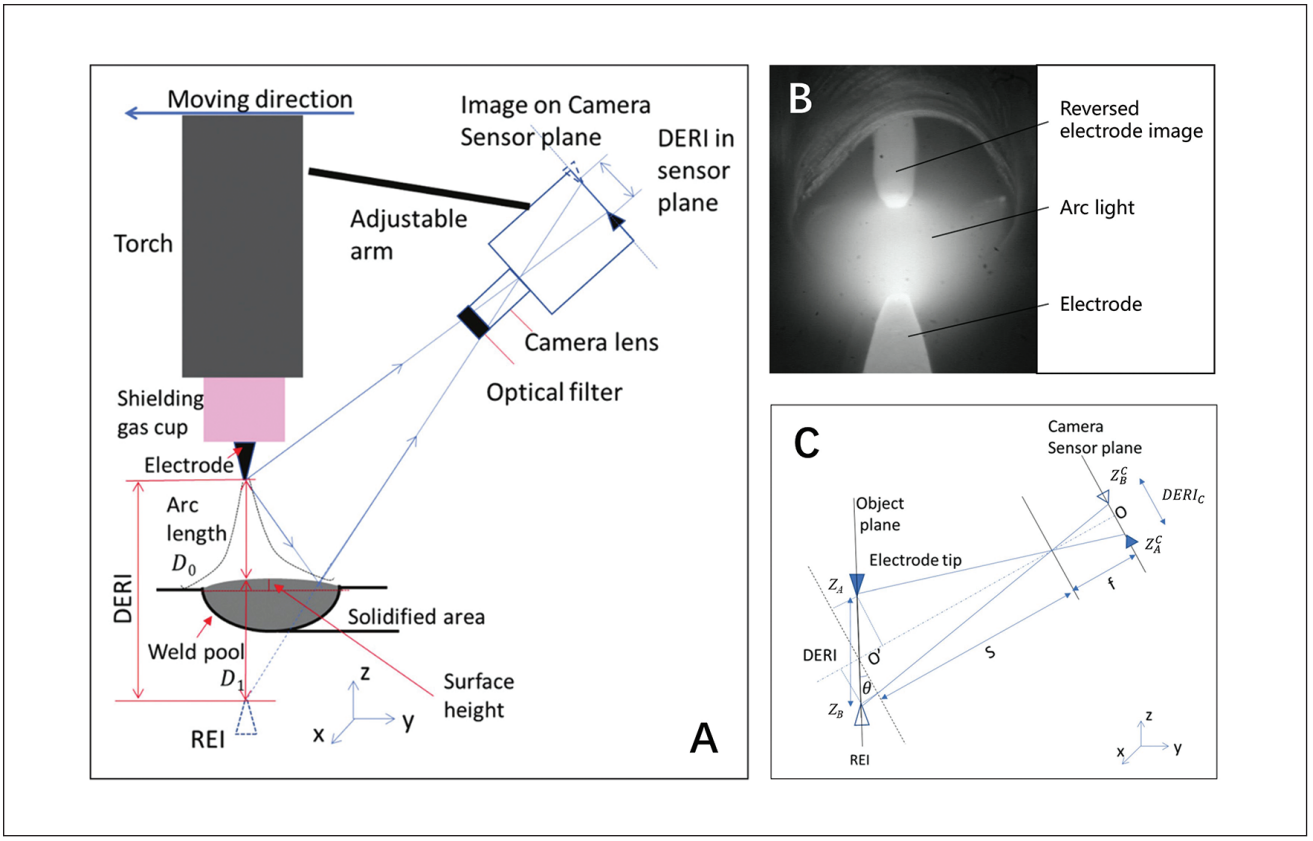

Fig. 1 — A — Diagram of passive vision monitoring system (Ref. 7); B — passive vision image of weld pool during GTAW; C — schematic of the pinhole camera model (Ref. 7).

process. Since the introduction of the REI, quite a few studies have been implemented to establish the relationship between REI and welding penetration state (Refs. 9, 10).

There have been many studies about the reflection of light on the weld pool surface: Chen et al. (Refs. 11, 12) calculated the 3D parameters of the weld pool surface according to the distribution of shadow; Zhang et al. (Refs. 13, 14) reconstructed the 3D weld pool surface by analyzing the reflected laser structure light. Based on the research about reflection on the weld pool surface and the feature of REI, this paper focused on the application of REI in monitoring of welding torch position and attitude. The main work from this paper includes the analysis of the geometry relationship between the weld pool and welding torch and the establishment of the REI-TPA model. The novel introduction of the REI-TPA model is an attempt to relate welding passive vision image to TPA, which contributes to automated welding and welding quality control.

The model can be applied to real-time monitoring and correction of TPA after further research and improvement of equipment accuracy. Compared with the methods in (Refs. 5, 6), the sensors used in the REI-TPA model are a camera and Hall sensors. There is no need to modify the welding torch, and the experimental setup is also relatively simple and low-cost.

The REI-TPA model also contributes to improving the accuracy of weld seam tracking and real-time correction of TPA. The laser vision sensor-based seam tracking technology has the advantages of a simple control structure and high precision (Ref. 15) and has become the most promising choice in practical welding (Ref. 16). In the laser vision sensor-based seam tracking system, distance exists between the laser stripe and welding point (Refs. 17–20), which will lead to a certain lag in the acquisition of information and the adjustment of welding torch posture. In the REI-TPA model, TPA is directly calculated with the features extracted from

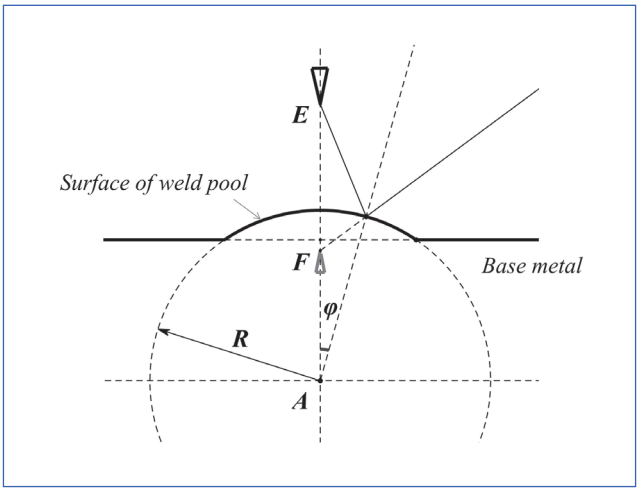

Fig. 2 — Imaging model of weld pool spherical surface.

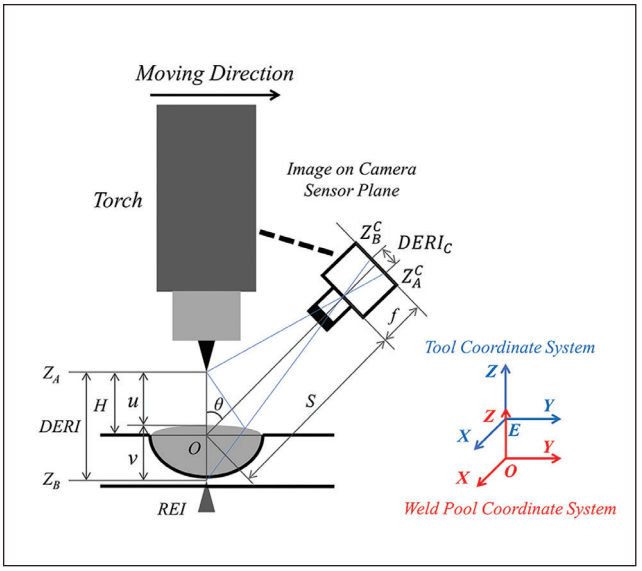

Fig. 3 — The diagram of the passive vision welding monitoring system and defined tool and weld pool coordinate system.

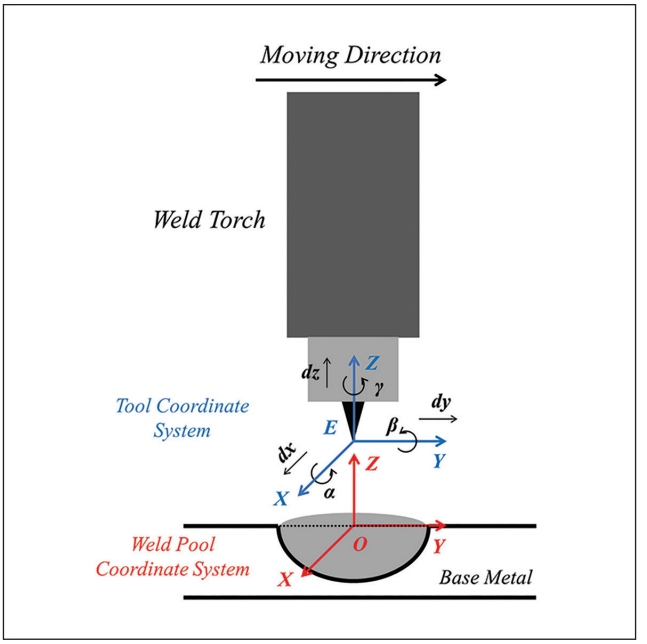

Fig. 4 — The position and attitude of TCS relative to WPCS.

the weld pool image at the welded point; therefore, almost no lag exists.

Besides the welding penetration state, the quality of the produced weld and TPA can be predicted simultaneously by combining the REI-TPA model with multi-information fusion and processing methods such as machine learning (Refs. 1, 21, 22) during the robotic welding process, which is an extension of the application and processing method of welding passive vision images.

Relationship Between REI and Welding Penetration

During GTAW, a virtual reversed electrode image was formulated on the surface of the weld pool due to the specular reflection. In Ref. 7, with the passive vision monitoring system shown in Fig. 1A, the images of the weld pool were collected, as shown in Fig. 1B. And the feature of REI was defined and extracted, then the surface height (SH) of the weld pool was calculated with:

$$\frac{-4 \cdot SH}{(d/2)^2 + SH^2} = \frac{1}{D_0} + \frac{1}{D_0 - DERI} \quad (1)$$

where d is the width of weld pool; D_0 is the distance between electrode tip and weld pool surface; $DERI$ is the distance between the electrode tip (Z_A) and the REI tip (Z_B), which was calculated with $DERI_C$, the distance between the electrode tip (Z_A^C) and the REI tip (Z_B^C) in the obtained passive vision image of weld pool, as shown in Fig. 1B:

$$DERI \approx \frac{DERI_C \cdot S}{f \cdot \cos\theta} \quad (2)$$

where S, f, θ were intrinsic and external parameters of the camera.

With Equations 1 and 2, the surface height of the weld pool was calculated in real time during GTAW. The welding penetration state was predicted with a deviation of the SH in Ref. 7. The feature of REI provided a new method to monitor the weld pool surface and 5 penetration states during the welding process, which was an important contribution to the intelligent welding manufacture. Based on the work of Chen et al. (Ref. 7), in this paper, the relationship between REI and TPA was studied, which was a supplement and expansion to the practical application and theoretical value of REI.

Imaging Model of Weld Pool Surface

In GTAW, the shape of the weld pool top surface is mainly determined by arc pressure, gravity, and surface tension. When the welding current is lower than 200 A, the surface depression of the weld pool can be almost ignored (Refs. 23, 24). In this research, the value of welding current was 120 A, which was much lower than 200 A. In this case, the arc pressure on the weld pool was much smaller than gravity and surface tension, the surface of the weld pool can be approximately regarded as a spherical surface (Ref. 7). Even if there are fluctuations on the surface of the weld pool, the computational error obtained with the REI-TPA model is small. This will be discussed in the Discussion section.

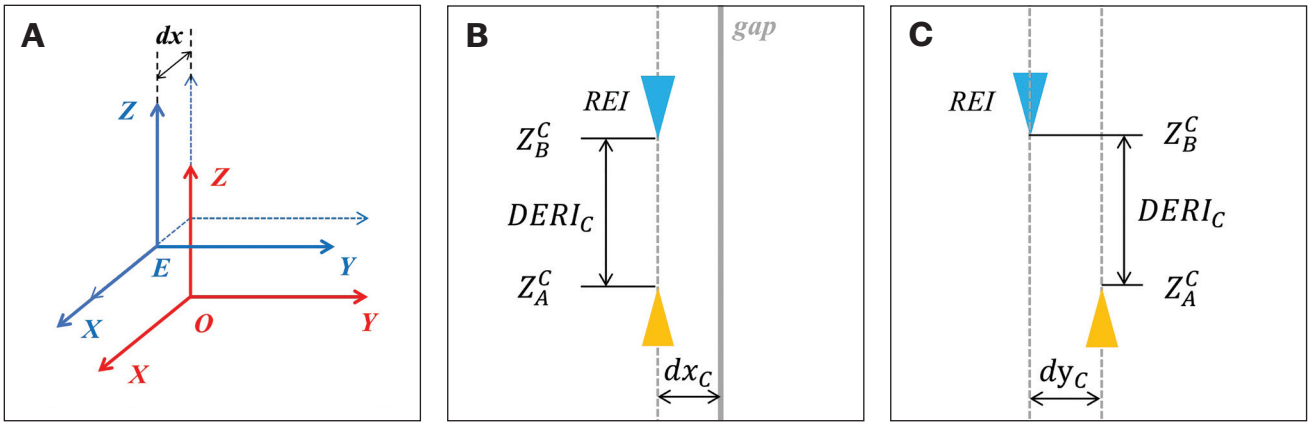

Fig. 5 — A — Position and attitude of TCS relative to WPCS when welding torch deviates from the point to be welded along the X-axis; B — schematic of the image obtained when welding torch deviates in X-axis direction; C — schematic of the image obtained when welding torch deflection around the Y-axis.

Considering the top surface of the weld pool as a spherical mirror, the REI was formed at the other side of weld pool surface, as shown in Fig. 2. In the figure, point *E* represents the tip of tungsten electrode; point *F* represents the tip of REI; point *A* represents the center of weld pool surface; φ is the angle between the main optic axis and normal line; and *R* is the radius of weld pool surface. The position of the REI tip, point *F*, can be calculated with:

$$\overline{AF} = \frac{\overline{AE} \cdot R}{2\overline{AE} \cdot \cos\varphi - R} \tag{3}$$

Expanding Equation 3 with the Mclaughlin formula and considering the angle φ as the independent variable:

$$\overline{AF} = \frac{R \cdot \overline{AE}}{2\overline{AE} - R} + \frac{(\overline{AE})^2 \cdot R}{(2\overline{AE} - R)^2} \cdot \varphi^2 + O(\varphi^4) \tag{4}$$

Since angle φ is usually small, the high-order terms in Equation 2 can be ignored, and Equation 4 becomes:

$$\overline{AF} = \frac{R \cdot \overline{AE}}{2\overline{AE} - R}$$

Note $u = \overline{AE} - R$, $v = R - \overline{AF}$, $f = R/2$, Equation 4 is transformed into:

$$\frac{1}{f} = \frac{1}{v} - \frac{1}{u} \tag{5}$$

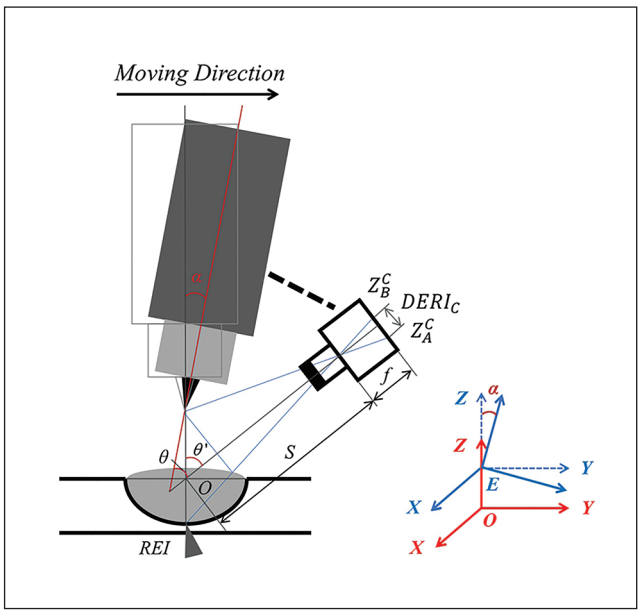

Fig. 6 — The position and attitude of TCS relative to WPCS when deflection occurs in the X-axis.

where *u* is the distance between the tip of the electrode and the top surface of the weld pool (i.e., object distance); *v* is the distance between the tip of REI and the top surface of the weld pool (i.e., image distance); and *f* is the focal length of weld pool surface.

Establishment of the REI-TPA Model

Tool Coordinate System and Weld Pool Coordinate System

The diagram of the passive visual monitoring system is shown in Fig. 3. The camera was fixed on the welding torch

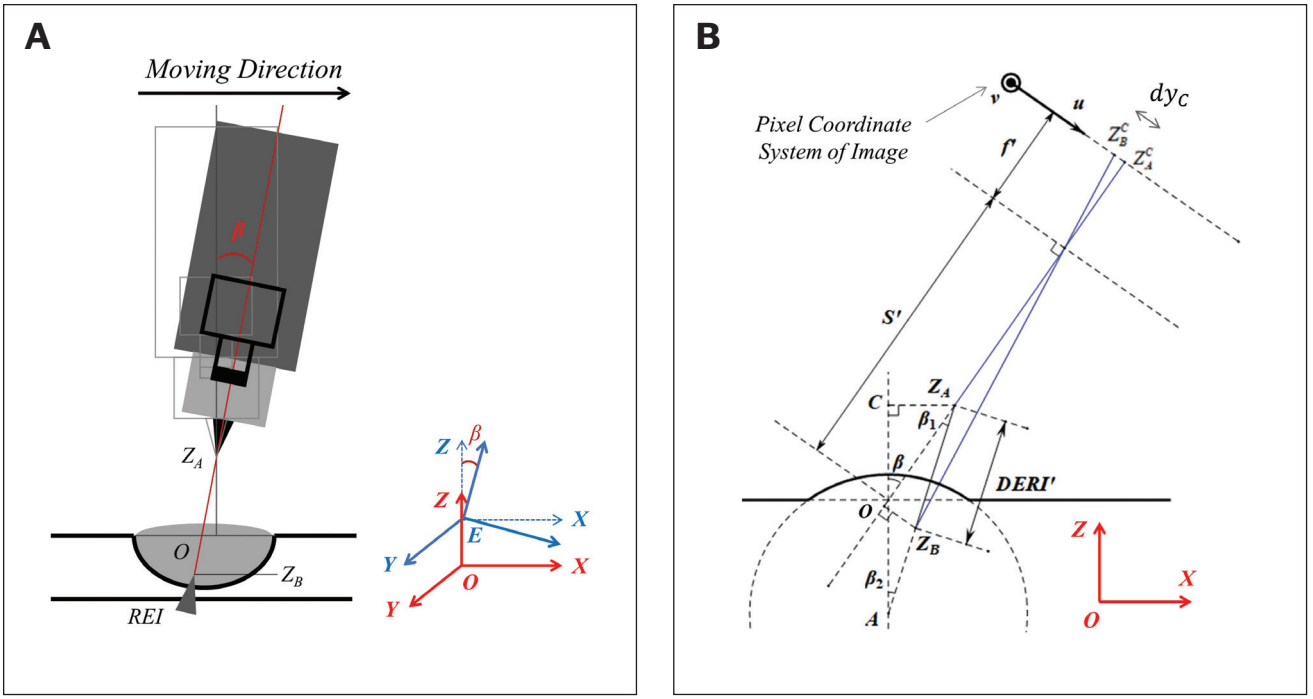

Fig. 7 — A — The position and attitude of TCS relative to WPCS when deflection occurs in the Y-axis; B — schematic of camera, weld pool, and welding torch projected in XOZ plane.

focusing on the weld seam. The setup angle of the camera relative to the welding torch was noted as θ, the focal length of the camera was noted as f, and the stand-off distance between the camera lens and the object plane was noted as S. To quantitatively describe the position and attitude of the welding torch relative to the weld seam, tool coordinate system (TCS) and weld pool coordinate system (WPCS) were established. The tip of the tungsten electrode was taken as the origin of TCS, and the origin of WPCS is the point to be welded on the weld seam. When the welding torch is in the normal pose, the attitude of the TCS and WPCS are the same with the Y-axis pointing to the welding direction, and the Z-axis perpendicular to the surface of the workpiece. The REI-TPA model describes the position and attitude of TCS relative to WPCS.

The position and attitude of TCS relative to WPCS can be described with displacement vectors (*dx, dy, dz*) and rotation vectors (α, β, γ), respectively, as shown in Fig. 4. *dx, dy, dz* represent the offset distance of TCS relative to WPCS along the X-Y-Z axis respectively; and α, β, γ represent the deflection angle of TCS relative to WPCS around X-Y-Z axis respectively. During the GTAW process, the direction of *dy* is the same as the walking direction of the welding torch, and γ has no influence on the welding process and quality of the produced weld. Besides, the change of *dy* and γ cannot be calculated with REI because the camera was fixed on the welding torch. Therefore, in the REI-TPA model, only the *dx*, *dz*, α, and β were included and calculated.

Welding Torch in Normal Pose

When the welding torch is in the normal pose, the relationship between *DERI* and *DERIC* was calculated with Equation 2 in Ref. 7:

$$DERI \approx \frac{DERI_C \cdot S}{f \cdot \sin\theta} \tag{6}$$

where *DERIC* can be calculated with the product of pixel number and pixel size in the obtained image. The pixel size of the camera used in this research is 6.8 × 6.8 µm. The difference between Equations 2 and 6 lies in the definition of setup angle θ.

The distance between the tip of the electrode and *REI*, *DERI*, can also be calculated with object distance, *u*, and image distance, *v*:

$$DERI = u + \frac{R \cdot u}{2u + R} \tag{7}$$

where *v* is expressed with *u* according to Equation 5, and u is equal to the length of the welding arc. The relationship between surface height (*SH*) and *R* is:

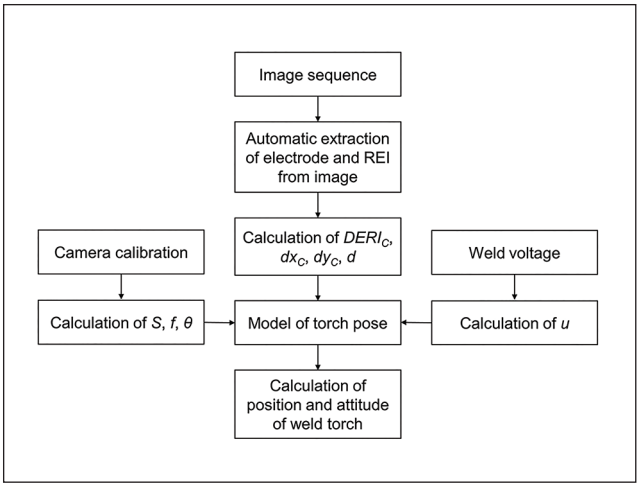

Fig. 8 — Flow chart of the calculation of welding torch position and attitude.

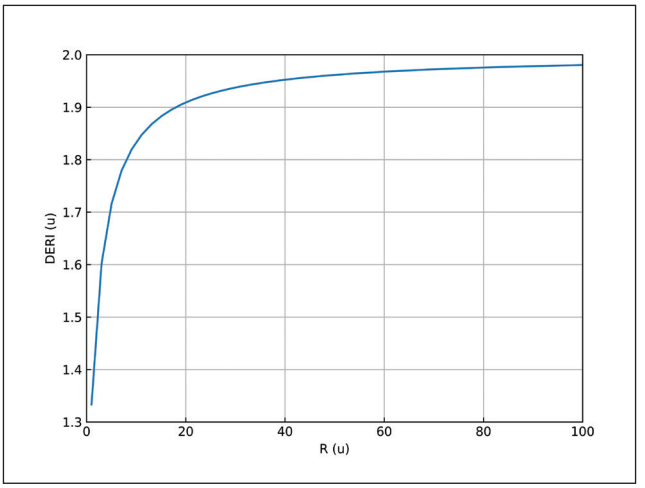

Fig. 9 — Relationship between DERI and R in Equation 7. DERI and R are expressed in unit of u.

$$R = \frac{d^2}{8SH} + \frac{SH}{2} \tag{8}$$

where d is the width of the weld pool, and $SH = H - u$. With Equations 6–8, *DERI* can be calculated with an imaging model of the weld pool surface and the imaging principle of the camera. Thus, the imaging model of the weld pool surface can be verified and the accuracy of camera calibration can be tested, the parameters (S, f, θ, *DERIC*, d, u, H) are required.

Welding Torch Offsets Along X-axis

When the welding torch deviates from the weld seam along X-axis, the position and attitude 9 of TCS relative to WPCS are shown in Fig. 5A. A schematic of the image captured by the camera under this condition is shown in Fig. 5B. According to the pinhole imaging principle of the camera, the offset distance in X-axis direction, dx, can be calculated with:

$$dx = \frac{S \cdot dx_C}{f} \tag{9}$$

where *dxC* represents the horizontal distance between the weld seam and the center line of REI and electrode, which can be calculated with the product of the pixel number and pixel size in the obtained image. Parameters (S, f, *dxC*) were required for the calculation of dx.

Welding Torch Deflects Around X-axis

When deflection occurs in X-axis, the position and attitude of TCS relative to WPCS are shown in Fig. 6. According to Fig. 6, the following equation was obtained

$$\theta' = \alpha + \theta$$

According to Equation 6,

$$\sin\theta' = \frac{DERI_C \cdot S}{DERI \cdot f}$$

Thus, the deflection angle of TCS in X-axis, α, can be calculated:

$$\alpha = \arcsin\left(\frac{DERI_C \cdot S}{DERI \cdot f}\right) - \theta \tag{10}$$

Parameters (S, f, θ, $DERI_C$, d, u, H) are required to calculate α.

Welding Torch Deflects Around Y-axis

When deflection occurs in the Y-axis, the position and attitude of TCS relative to WPCS are shown in Fig. 7A, and the diagram of the obtained image in the camera is shown in Fig. 5C. To calculate the deflection angle around Y-axis, the camera, weld pool, and welding torch were projected to XOZ plane, as shown in Fig. 7B. According to Fig. 7B:

$$\frac{DERI' \cdot \sin\beta_1}{dy_C} \approx \frac{S'}{f'}$$

where $DERI' = DERI \cdot cos\theta$, $S' = S \cdot cos\theta$, $f' = f \cdot cos\theta$, dy_c represents the horizontal distance between the center line of REI and electrode, as shown in Fig. 5C. In ΔACZ_A:

Table 1 — The REI-TPA Model and the Required Parameters of Each Equation

Torch Position and Attitude	Calculation Formula	Parameters Required
Normal	$DERI \approx \frac{DERI_C \cdot S}{f \cdot \sin\theta}$, $DERI = u + \frac{R \cdot u}{2u+R}$	*S*, *f*, θ, *DERIc*, *d*, *u*, *H*
Offset along X-axis	$dx = \frac{S \cdot dx_C}{f}$	*S*, *f*, dx_C
Deflection around X-axis	$\alpha = \arcsin(\frac{DERI_C \cdot S}{DERI \cdot f}) - \theta$	*S*, *f*, θ, $DERI_C$, *d*, *u*, *H*
Deflection around Y-axis	$\beta = \arctan\frac{S \cdot dy_C}{f \cdot (1-a) \cdot DERI \cdot \cos\theta}$	*S*, *f*, θ, *d*, *u*, dy_C, *H*
Offset along Z-axis	$dz = du$	*du*

$$\tan\beta_1 = \frac{(1-a)\cdot\tan\beta}{1 + a\cdot\tan^2\beta}$$

where $a = \overline{OC} / \overline{AC} \approx H / (R + H - u)$. Since the angle β is usually small, the above equation becomes:

$$\tan\beta_1 = (1-a)\cdot\tan\beta$$

Since the angle β_1 is quite small, $\sin\beta_1 \approx \tan\beta_1$. Thus, the deflection angle in Y-axis, β, is calculated:

$$\beta = \arctan\frac{S \cdot dy_C}{f \cdot (1-a) \cdot DERI \cdot \cos\theta} \quad (11)$$

Parameters (*S*, *f*, *θ*, *d*, *u*, dy_C, *H*) are required to calculate β.

Welding Torch Offsets Along Z-axis

When an offset occurs in the Z-axis, the length of the welding arc will change accordingly. Therefore, the offset of the welding torch along the Z-axis direction can be calculated with the variation of arc length:

$$dz = du \quad (12)$$

To calculate the offset in the Z-axis, the change of arc length, *du*, is required.

REI-TPA Model

The REI-TPA model is composed of Equations (6, 7, 9–12). The equations and the required parameters of each equation are summarized in Table 1. The required parameters can be divided into four categories: (1) S, f, *θ* are the intrinsic and external parameters of camera, which can be obtained with camera calibration; (2) $DERI_C$, dx_C, dy_C, and *d* are parameters extracted from the passive vision images of weld pool, which can be calculated with the product of pixel number and pixel size in the obtained image; (3) u is equal to the arc length during welding process, which can be calculated with welding voltage; (4) H is a constant, which was preset before welding.

Discussion

Procedure for Calculating the TPA with the REI-TPA Model

The procedure for calculating the TPA with the REI-TPA model is presented in Fig. 8. Before the welding experiment, camera calibration was performed to determine the intrinsic and external parameters, (*S*, *f*, θ), of the camera. To obtain the parameters ($DERI_C$, dx_C, dy_C, *d*), a robust algorithm should be developed to extract the contours of the electrode and REI 13 from the passive vision image of the weld pool. The arc length, *u*, would be calculated using welding voltage with the linear relationship between welding voltage and arc length. Then, input the obtained parameters into the REI-TPA model, and the position and attitude of the welding torch could be obtained. The process can be summarized into three parts: (1) collecting welding data including welding current and current, image of the weld pool; (2) designing a robust algorithm to extract required parameters from the collected

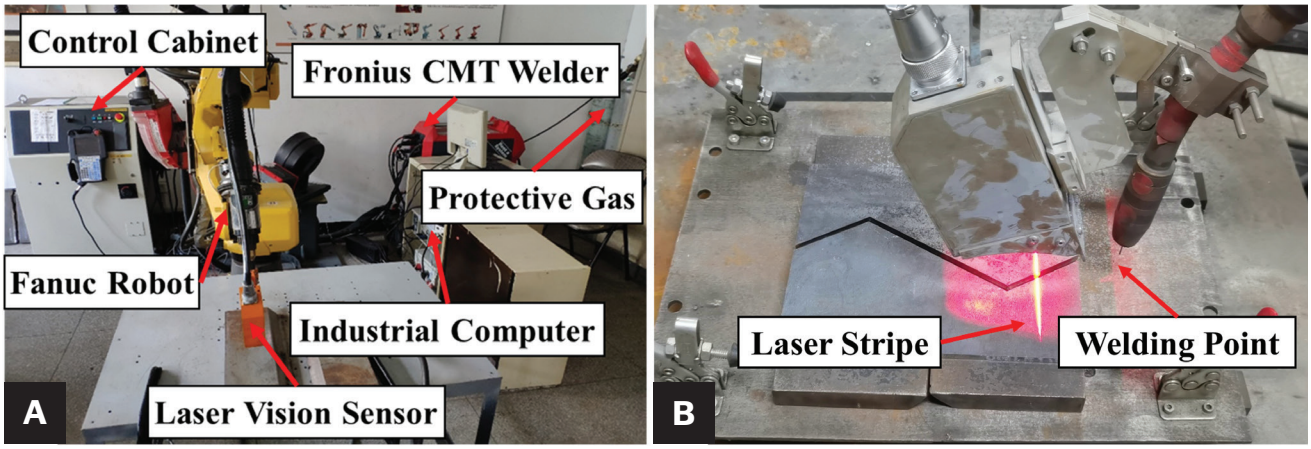

Fig. 10 — A — Laser vision-based seam tracking system in Ref. 13; B — relative position between weld torch and laser stripe in seam tracking system.

data; (3) inputting the parameters into the REI-TPA model to auto-calculate TPA. These three parts and the validation of the REI-TPA model will be presented in the subsequent research.

Shape Changing of Weld Pool

During the welding process, fluctuations may occur on the surface of the weld pool due to the influence of factors including the filler wire, arc pressure, local deformation of the workpiece, etc. The shape-changing of the weld pool would lead to the variation of the radius *R*. In Equation 7, the variation of the parameter *R* transfers to the parameter *DERI*, affecting the computational result of the REI-TPA model through Equations 10 and 11. Thus, in the REI-TPA model, only the calculation of the deflection angle around the X and Y axis would be affected by the fluctuations of the weld pool.

In Equation 7, expressing *DERI* and *R* in unit of *u*, the relationship between *DERI* 14 and *R* is shown in Fig. 9. According to Fig. 9, when $R > 20u$, the variation of parameter *R* has a low impact on the parameter *DERI*. Since the value of *R* is usually much larger than *u* during the welding process, the slight fluctuation of the weld pool has little influence on the computational result of the REI-TPA model. When the weld pool fluctuates violently, the value of the local radius may be close to or less than the value of *u*. In this case, the accuracy of the computational result will decrease.

Feature of the REI-TPA Model

On the monitoring of TPA, compared with other methods using sensors such as angle sensors (Ref. 5), rotating arc sensor (Ref. 6), etc., the sensors used in the REI-TPA model are a camera and Hall sensors, so there is no need to modify the welding torch. The experimental setup is also relatively simple and low-cost. Besides, with the model, the overall position and attitude of the welding torch can be obtained.

In addition to the automatic calculation of TPA, the REI-TPA model also contributes to improving the accuracy of weld seam tracking. In the seam tracking process during the robotic welding process, to obtain the position information of the seam, the laser sensor is set in front of the welding torch (Refs. 17–20), as shown in Fig. 10. There is a distance between the laser stripe and welding point, which will lead to a certain lag in the acquisition of information and the adjustment of welding torch posture. While in the REI-TPA model, the images are collected exactly under the welding torch. The TPA is directly calculated with the features extracted from the weld pool image at the welded point, therefore, almost no lag exists.

The REI-TPA model can be combined with multi-information fusion and processing methods such as machine learning (Refs. 1, 21, 22) during the welding process. Thus, multi-information including welding penetration state, quality of the produced weld, and TPA can be predicted simultaneously, which is an extension to the application and processing method of welding passive vision image.

The REI-TPA model also has certain limitations: the calculation of the deflection angle is sensitive to the error of the required parameters due to the inverse trigonometric function in Equations 10 and 11. Thus, relatively high accuracy of the Hall sensor and camera is required.

Conclusions

Based on the research of REI on monitoring of weld pool surface and penetration state (Refs. 7–9), this paper focuses on the application of REI in monitoring welding torch position and attitude. In this paper, the REI-TPA model was established by considering the surface of the weld pool as a spherical mirror. With the REI-TPA model, the position and attitude of the welding torch can be calculated with parameters including welding voltage, the geometry of weld pool, and relative distance between the tip of REI and electrode in the obtained image of the weld pool. Offset distance and deflection angle of the welding torch are relative to the correct position and attitude can be calculated in real time using the REI-TPA model. And real-time monitoring and correction of TPA can be realized, the REI-TPA model also contributes to improving the accuracy of weld seam tracking.

The REI-TPA model provides a convenient method to monitor the position and attitude of the welding torch, which is of significance to automated welding and welding quality control. The REI-TPA model is a supplement to the welding visual sensing technology and an expansion to the acquisition and processing of multi-source information during the welding process.

As a sequel to this paper, the second part of the continuing research will focus on the adaptive extraction of the required parameters and the experimental validation of the REI-TPA model (Ref. 25). In the next research, the REI-TPA model will be validated 16 with bead-on-plate welding experiments on S304 stainless steel plate, contours of the REI and electrode as well as the weld pool geometry will be extracted with a developed robust algorithm, and the application of the REI-TPA model in seam tracking during robotic welding process will be discussed.

Acknowledgments

This work is partly supported by the National Natural Science Foundation of China under Grant No. 61873164.

References

1. Zhang, Y., Wang, Q., and Liu, Y. 2021. Adaptive intelligent welding manufacturing. *Welding Journal* 100(1): 63-83.

2. Chen, S. 2015. On Intelligentized welding manufacturing. *The Advances in Intelligent Systems and Computing* 363: 3-34.

3. Chen, S. and Lv, N. 2014. Research evolution on intelligentized technologies for arc welding process. *Journal of Manufacturing Processes* 16(1): 109-122.

4. Zhang, G., Shi, Y., and Gu, Y., et al. 2017. Welding torch attitude-based study of human welder interactive behavior with weld pool in GTAW. *Robotics and Computer-Integrated Manufacturing* 48: 145-156.

5. Zhang, W., Xiao, J., and Chen, H., et al. 2014. Measurement of three-dimensional welding torch orientation for manual arc welding process. *Measurement Science and Technology* 25(3): 035010.

6. Le, J., Zhang, H., and Chen, X. 2018. Realization of rectangular fillet weld tracking based on rotating arc sensors and analysis of experimental results in gas metal arc welding. *Robotics and Computer-Integrated Manufacturing* 49: 263-276.

7. Chen, Z., Chen, J., and Feng, Z. 2017. Monitoring weld pool surface and penetration using reversed electrode images. *Welding Journal* 96(10).

8. Chen, Z., Chen, J., and Feng, Z. 2019. 3D weld pool surface geometry measurement with adaptive passive vision images. *Welding Journal* 98(12): 379-s to 386-s.

9. Chen, Z., Chen, J., and Feng, Z. 2018. Welding penetration prediction with passive vision system. *Journal of Manufacturing Processes* 36: 224-230.

10. Feng, Y., Chen, Z., and Wang, D., et al. 2019. DeepWelding: A deep learning enhanced approach to GTAW using multisource sensing images. *IEEE Transactions on Industrial Informatics* 16(1): 465-474

11. Zhao, D., Yi, J., and Chen, S., et al. 2003. Extraction of three-dimension parameters for weld pool surface in pulsed GTAW with wire filler. *Journal of Manufacturing Science and Engineering* 125(3): 493-503.

12. Du, Q., Chen, S., and Lin, T. 2006. Inspection on shape of weld based on shape from shading. *International Journal of Advanced Manufacturing Technology* 27: 667-671

13. Song, H., and Zhang, Y. 2008. Measurement and analysis of three-dimensional specular gas tungsten arc weld pool surface. *Welding Journal* 87(4): 85-s to 95-s.

14. Wang, Z., Zhang, Y., and Yang, R. 2013. Analytical reconstruction of threedimensional weld pool surface in GTAW. *Journal of Manufacturing Processes* 15(1): 34-40.

15. Agapakis, J., Katz, J., and Koifman, M., et al. 1986. Joint tracking and adaptive robotic welding using vision sensing of the weld joint geometry. *Welding Journal* 65(11).

16. Cheng, Y., Yu, R., and Zhou, Q., et al, 2021. Real-time sensing of gas metal arc welding process–A literature review and analysis. *Journal of Manufacturing Processes* 70: 452-469.

17. Xiao, R., Xu, Y., and Xu, F., et al. 2023. LSFP-tracker: an autonomous laser stripe feature point extraction algorithm based on iamese network for robotic welding seam 18 tracking. *IEEE Transactions on Industrial Electronics*: 1-10.

18. Wei, S., Ma, H., and Lin, T., et al. 2010. Autonomous guidance of initial welding position with" single camera and double positions" method. *Sensor Review* 30(1): 62.

19. Muhammad, J., Altun, H., and Abo-Serie, E. 2017. Welding seam profiling techniques based on active vision sensing for intelligent robotic welding. *The International Journal of Advanced Manufacturing Technology* 88(1): 127-145.

20. Xiao, R., Xu, Y., and Hou, Z., et al. 2019. An adaptive feature extraction algorithm for multiple typical seam tracking based on vision sensor in robotic arc welding. *Sensors and Actuators A: Physical* 297: 111533.

21. Chen, B., Wang, J., and Chen, S. 2010. Prediction of pulsed GTAW penetration status based on BP neural network and DS evidence theory information fusion. *The International Journal of Advanced Manufacturing Technology* 48(1): 83-94.

22. Zhang, Z., Chen, H., and Xu, Y. 2015. Multisensor-based real-time quality monitoring by means of feature extraction, selection and modeling for Al alloy in arc welding. *Mechanical Systems and Signal Processing* 60: 151-165

23. Lin, M., and Eagar, T. 1985. Influence of arc pressure on weld pool geometry. *Welding Journal* 64(6): 163-s to 169-s.

24. Zhang, Y., Cao, Z., and Kovacevic, R. 1996. Numerical analysis of fully penetrated weld pools in gas tungsten arc welding. *Proceedings of the Institution of Mechanical Engineers, Part C: Journal of Mechanical Engineering Science* 210(2): 187–195.

25. Fu, Y., Liu, Q., Xiao, R., and Chen, S. B. Monitoring Welding Torch Position and Posture Using Reversed Electrode Images – Part II Experimental and Analysis for the REI-TPA Model. Submitted to the *Welding Journal*.

YU FU and **SHANBEN CHEN** (*sbchen@sjtu.edu.cn*) are with Shanghai Jiao Tong University, Shanghai, People's Republic of China.